LA-UR-96-2580

Hadron Distributions - Recent Results from the CERN Experiment NA44

Nu Xu *for the NA44 Collaboration* [a]
I.G. Bearden, H. Bøggild, J. Boissevain, J. Dodd, B. Erazmus, S. Esumi, C.W. Fabjan, D. Ferenc, D. E. Fields, A. Franz, J.J. Gaardhøje, O. Hansen, D. Hardtke, H. van Hecke, E.B. Holzer, T. Humanic, P. Hummel, B.V. Jacak, R. Jayanti, M. Kaneta, M. Kopytine, M. Leltchouk, T. Ljubicic, B. Lörstad, N. Maeda, A. Medvedev, M. Murray, S. Nishimura, H. Ohnishi, G. Paic, S.U. Pandey, F. Piuz, J. Pluta, V. Polychronakos, M. Potekhin, G. Poulard, A. Sakaguchi, J. Simon-Gillo, J. Schmidt-Sørensen, W. Sondheim, M. Spegel, T. Sugitate, J. P. Sullivan, Y. Sumi, W.J. Willis, K.Wolf, N. Xu, and D.S. Zachary [b]

[a]Los Alamos National Laboratory, Los Alamos, NM 87545, U.S.A.

[b] NBI-LANL-Columbia-CERN-Nantes-Hiroshima-Zagreb-OSU-Lund-TexasA&M-BNL

Proton distributions at midrapidity have been measured for 158A·GeV Pb+Pb collisions in the focusing spectrometer experiment NA44 at CERN. A high degree of nuclear stopping is found in the truly heavy ion collisions. Systematic results of single particle transverse momentum distributions of pions, kaons, and protons, of 200A·GeV S+S and 158A·GeV Pb+Pb central collisions will be addressed within the context of thermalization. By comparing these data with thermal and transport models, freeze-out parameters such as the temperature parameter T_{fo} and mean collective flow velocity $\langle\beta\rangle$ are extracted. Preliminary results of the particle ratios of K^-/K^+ and $\bar{p}/p$ are discussed in the context of cascade models of RQMD and VENUS.

1. INTRODUCTION

The physics motivation of ultrarelativistic heavy-ion collisions is to prepare nuclear matter with high baryon and energy densities, and we hope to reach the new form of matter called quark-gluon plasma. By studying the decay of the system, we will gain knowledge of strong interactions under these extreme conditions and shed light on the puzzle of quark confinement.

Heavy-ion collisions, from beginning to end, can be roughly divided into to three phases: (i) Incoming nucleons interact with each other and lose energy to produce secondary particles and induce the transverse motion which is almost zero at the beginning. A fireball with high energy and particle densities is created; (ii) Due to the large number of rescatterings, the system approaches thermal (or even chemical) equilibrium and collective expansion starts to develop. Within the framework of a thermal model, it is possible to describe an ensemble of such collisions with a small set of parameters: temperature T, collective velocity β, and chemical potentials (μ_q, μ_s); (iii) After awhile, when the system becomes dilute, interactions among particles become less frequent and eventually cease. At this moment, particles become free-streaming. Strictly speaking, there are no precise boundaries between the three stages: initial, thermodynamic, and freeze-out. The collision process evolves continuously. The fireball created in the collision contains a finite number of particles, and its lifetime and spatial extent are also limited. Furthermore, due to the finite interaction cross section among hadrons, statistically the freeze-out occurs from the outside toward the inside of the fireball. To some extent, one may imagine that free-streaming hadrons are evaporated from the fireball surface.

All experimental observables emerge at freeze-out. It is our task to understand the collision dynamics at earlier stages by analyzing the final particle distributions. In this paper, after a brief description of the NA44 experiment, we will first discuss the proton rapidity distributions of the 158A·GeV Pb+Pb central collisions. Physics of nuclear stopping in these truly heavy-ion collisions will be addressed. Then, the transverse momentum distributions of pions, kaons, and protons from p+p, S+S, and Pb+Pb collisions are discussed. From this study, we will be able to define a common freeze-out temperature parameter T_{fo}.

2. CERN EXPERIMENT NA44

The NA44 spectrometer is designed to measure one- and two-particle distributions of charged hadrons near the center of mass rapidity ($y_{mid} \approx 3$) over a transverse momentum range of $0 \leq p_T \leq 1.6$ GeV/c. Threshold Cherenkov counters and time-of-flight (TOF) scintillator hodoscopes are used for particle identification and momentum reconstruction. The TOF resolution is about 100 ps and momentum spread is about $\delta p/p \approx 0.5\%$. The interaction trigger is provided by two scintillator paddles placed downstream of the target. For AA collisions, the trigger cross section is approximately $\sigma_{trig}/\sigma_{geom} \approx 10\%$, while for pA collisions a minimum bias trigger was used. More details of the spectrometer can be found elsewhere [1,2].

3. RESULTS AND DISCUSSION

3.1. Proton Rapidity Distributions

The goal of heavy-ion physics is to reach high particle and energy densities. Nucleon distributions yield information on nuclear stopping in nucleus-nucleus collisions, which provides a measure of how much initial kinetic energy is deposited into the system during the collisions [3]. The higher the nuclear stopping, the more initial energy is converted into excitation of the system. For p+p collisions at a beam energy of $E_{beam} \approx 200$ GeV, the proton rapidity distribution shows two distinct peaks near beam and target rapidity, i.e., baryon stopping and production at midrapidity is small. Experimentally it has been found [4] that nuclear stopping in symmetric S+S collision is higher than that of a p+p collision. For the p-nucleus collisions [5] significant nuclear stopping was already inferred from the analysis of the final proton rapidity distributions of 100 GeV/c p+Pb collisions [6]-[10].

In November 1994, 158A·GeV ($\sqrt{s} \approx 17.5$A·GeV) lead beams were delivered from the CERN Super Proton Synchrotron (SPS). The data presented here were taken during the '94 run period. Figure 1 shows the proton rapidity distribution where filled circles are measured data and open circles are the same data points mirrored around $y_{mid} = 2.9$. The error bars are statistical only. The systematic errors on the proton rapidity density are dominated by errors in centrality selection, the pion veto correction, and total number of beam particles. These contribute about 25%, 15%, and 10% systematic uncertainties to dN/dy, respectively. Assuming there are no correlations among the errors and adding them in quadrature, the overall systematic uncertainties in the final rapidity distribution dN/dy are 26.8% and 32.7% for 4 and 8 GeV/c settings, respectively. These errors are shown as brackets in the figure. Unlike in proton-proton and light ion collisions, we observe a large proton rapidity density around midrapidity, indicating that the incoming projectile and target protons undergo a large rapidity shift.

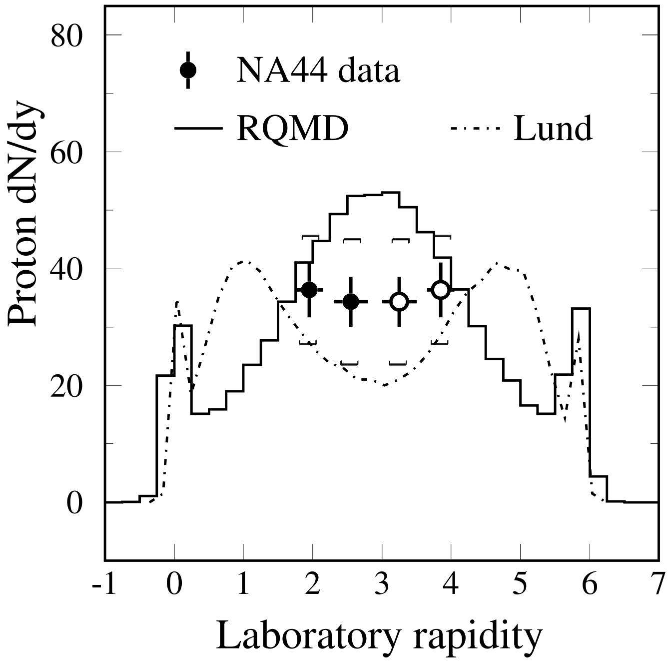

Figure 1. Proton rapidity distributions from central Pb+Pb collisions. The open circles are the mirrored points about y_{mid} = 2.9. Statistical errors are shown as bars and the overall systematic errors are shown as brackets. The RQMD calculation is shown as a solid line. The FRITIOF model prediction is shown as a dot-dashed line.

The RQMD (v1.08) model [11] proton rapidity distributions are shown in Fig. 1 as a solid line. Protons from decays, primarily from Λ's, have been included in the calculation. Without these decayed protons the maximum RQMD dN/dy would be about 38. A realistic centrality cut, measured by the T_0 counter, was used in the model calculation. Spectator protons appear at target and projectile rapidity, and constitute about 16% of the total protons. This is consistent with the impact parameter cut used in the calculation.

In contrast to the RQMD results, the FRITIOF model [12] predicts a dip at midrapidity in net proton production from central Pb+Pb collisions. The dot-dashed line in Fig. 1 shows four distinct peaks in the distribution. In addition to the spectator peaks, the struck protons are visible as peaks about one unit away from the spectators. This is a low-stopping or transparency result for heavy-ion collisions. The model predicts such a small rapidity shift in heavy-ion collisions because it assumes that the scattered (or undressed [13]) nucleons suffer no additional collisions and eventually materialize outside the collision zone.

The analysis of p+Pb→p collisions [9] shows that a large amount of energy can be dissipated. One consequence of this is that outgoing protons can undergo rather large rapidity shifts compared to those in p+p collisions. Any phenomenological model that provides a sufficient rapidity-shift mechanism will fit the experimental p+A and A+A data well [14–16]. However, these models do not answer detailed questions about how a fast nucleon or parton loses energy inside the nuclear medium or what role gluons play in such high energy collisions.

Given the rather large systematic uncertainties in the dN/dy measurements a definitive conclusion on the amount of stopping cannot be reached. By combining this measurement with slope parameters of pions, kaons, and protons, and the Coulomb effect (see discussions below), free of such systematic errors, the result is consistent with the scenario of high nuclear stopping in these Pb+Pb collisions.

3.2. Coulomb Effect in Pion Distributions

In truly heavy-ion collisions, Pb+Pb, the large amount of positive charge in the system can introduce additional distortions of the particle final distributions. The Coulomb interaction between the emitted particles and the charged system influences the final particle spectra. Though it represents a background to the study of other phenomena at low p_T, it is important to understand this before discussing new physics from heavy-ion collisions. In addition, observation of the Coulomb interaction may provide information on the collision dynamics, such as collective expansion. In this section, we investigate the Coulomb interaction through the ratio of negative to positive pions produced in high energy heavy-ion collisions at the CERN SPS.

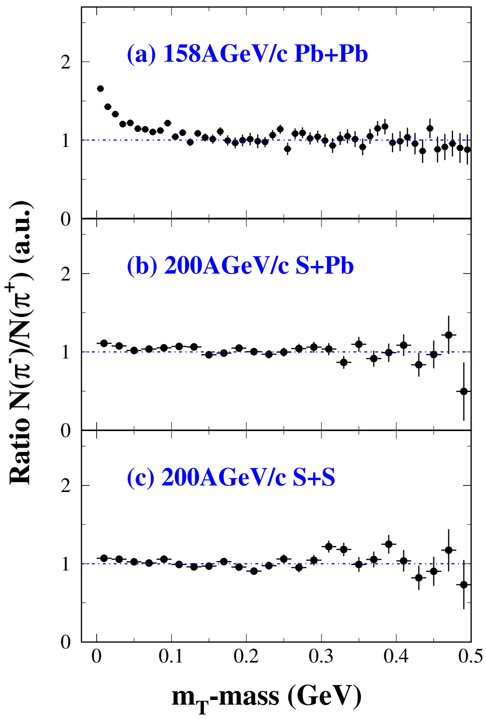

Figure 2. Experimental ratios N(π^-)/N(π^+) from (a) 158A·GeV Pb+Pb, (b) 200A·GeV S+Pb, and (c) 200A·GeV S+S collisions. The data are arbitrarily normalized to unity at high m_T.

Identified charged pions were used to construct the ratio π^-/π^+ as a function of transverse kinetic energy (m_T − mass).[1] The result is shown in Fig. 2 where (a) shows the ratio π^-/π^+ from 158A·GeV Pb+Pb central collisions [17]. A pronounced enhancement in the π^-/π^+ ratio at low transverse kinetic energy is evident. For comparison, the ra-

[1] $m_T = (p_T^2 + \mathrm{mass}^2)^{1/2}$.

tios π^-/π^+ from 200A·GeV S+Pb [18] and S+S collisions are shown in Fig. 2(b) and (c), respectively. These data were taken with the same spectrometer and similar analysis methods were used. The centralities of the data discussed here are 10±2%, 14±2%, and 15±1.5% of total cross section for S+S, S+Pb and Pb+Pb collisions, respectively. Unlike the case for Pb+Pb collisions, the ratios from the lighter collision systems are found to be almost flat. A similar result was reported [19] from lower energy collisions.

It is interesting to test whether the effect observed in the ratio π^-/π^+ might be caused by hadronic interactions. We used the cascade model RQMD (v1.08) [11] to calculate the charged pion distributions in central Pb+Pb collisions. RQMD is a microscopic transport model, and includes the physics of string-string and hadron-hadron interactions including resonance effects. However, the Coulomb interaction is not considered. The result of the calculated ratio π^-/π^+ is shown in Fig. 3 as a dashed line. A realistic centrality selection and spectrometer acceptance were used in the model calculation. Long-lived hyperons (Λ and Σ, for example) were included in the calculation. The slight excess of the π^- above π^+ in this calculation is mainly due to Λ decays, where about 25% of the pions from decays survive the reconstruction. It can be seen from the figure that the calculated ratio has an enhancement as $p_T \to 0$. The peak is about 1.1, much smaller than the data. Without the long-lived hyperon decays, RQMD predicts a flat distribution.

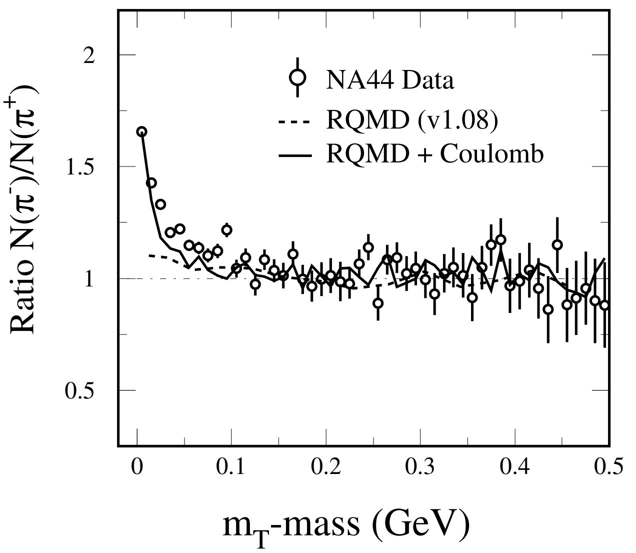

Figure 3. Data (filled circles) compared with results from the RQMD (v1.08) predictions (dashed line) where the hyperon decay probabilities and the spectrometer acceptance are included in the model calculation and the result (solid line) of RQMD + Coulomb calculations.

The solid line in Fig. 3 is the prediction of the RQMD plus Coulomb calculation [20, 21]. As an afterburner, the longitudinal co-moving charge of $Z_{eff} = 40$ was used in the calculation. Although the solid curve does not fit to the measured points exactly, the agreement between data and the calculation is remarkable. A similar result was also obtained from a hydrodynamic model calculation [22]. Note that the calculation is very sensitive to the value of the net charge and Z_{eff}= 40 per unit rapidity is consistent with observed proton dN/dy at the midrapidity region. In addition, the calculated ratios of K^-/K^+ and $\overline{p}/p$ are flat with respect to the transverse momentum, which is again consistent with our observation.

We conclude that the observed enhancement at p_T near zero in the π^-/π^+ ratio is mostly caused by the Coulomb interaction rather than hadronic interactions.[2] Both the NA44 recent measurement and RQMD show a large number of protons around midrapidity indicating a large amount of positive charge in the central region. This supports the assertion that the effect observed in the π^-/π^+ ratio is indeed due to Coulomb interactions plus some contributions from hyperon decay. The fact that a large amount of positive charge around the midrapidity region is due to the high nuclear stopping discussed in the previous section.

3.3. Transverse Momentum Distributions

In high energy collisions, it is well known that at high p_T limit, a transverse kinetic energy distribution can be represented by a simple exponential function: $exp(-m_T/T)$.[3] Here T is the slope parameter. The magnitude of the slope parameter provides information on temperature (random motion in local rest frame) and collective transverse flow, and any deviation from the exponential distribution may signal new physics such as the low p_T enhancement, medium effect [23], etc.

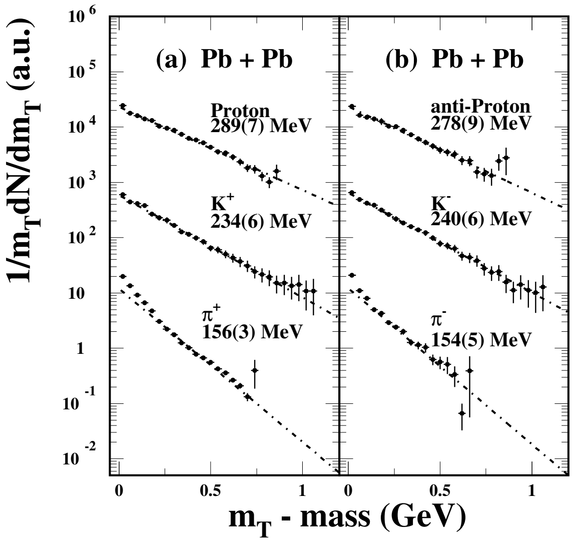

Figure 4. NA44 preliminary transverse momentum distributions for pions, kaons, and protons.

In the following, we will discussion the pion, kaon, and proton transverse kinetic energy distributions from p+p, S+S, and Pb+Pb collisions. These distributions were all extracted around midrapidity. The beam energy of the proton beam is 450 GeV, $y_{NN} = 3.44$; for the Sulphur beam it is 200A·GeV with $y_{NN} = 3.03$; and for the lead beam 158A·GeV with $y_{NN} = 2.91$.

Figure 4 shows the transverse kinetic energy distributions of charged pions, kaons, and protons from Pb+Pb central collisions. The dashed lines are the exponential fits to the distributions and the fitted slope parameters are indicated in the figure.[4]

---

[2] However, one should bear in mind that the RQMD model is a classical hadronic transport model. Possible new physics, such as medium effects or chiral symmetry restoration, are not included.

[3] Note that an exponential shape is only consistent with a thermal distribution, but is not necessarily a proof of thermalization.

[4] To avoid the distortion caused by high mass resonances in the pion spectra, the fit started from $m_T -$

First of all, the exponential functions fit to the data well except for pions in the low p_T region, where one expects the resonances decays. The slope parameters increase as particle mass increases and this is independent of the sign of the particles. To make this point clear, we summarize the slope parameters of pions, kaons, and protons from three collision systems: p+p [24] ($\sqrt{s} \approx 23$ GeV), S+S ($\sqrt{s} \approx 19.4$A·GeV), and Pb+Pb ($\sqrt{s} \approx 17.3$A·GeV) in Fig. 5.

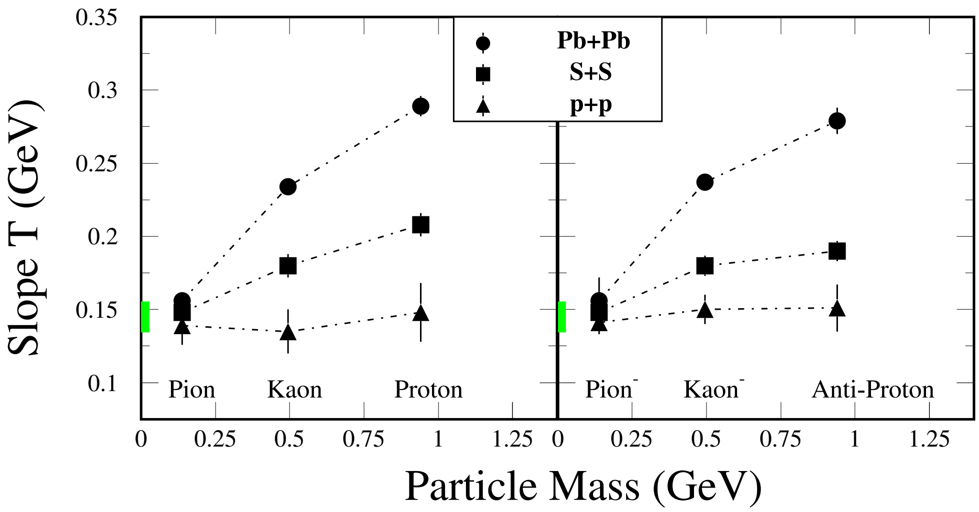

Figure 5. Slope parameter T as a function of particle mass. The p+p results are taken from Ref. [24].

A distinct difference between the results of the elementary p+p collision and heavy-ion collisions can be seen in the slope parameters. While the slope parameters of p+p collisions (triangles) remain flat as a function of the particle mass, these parameters from heavy ion collisions increase as the mass increases. Furthermore, for a given mass, the heavier the colliding system, the higher the slope parameter. It is also interesting to observe that all curves converge to a point about $T_{fo} \approx 145 \pm 15$ MeV, as indicated by the shaded bars in Fig. 5. In hydrodynamics, matter flows, i.e., all particles flow at a same collective velocity. Classically, the collective kinetic energy will then depend on the particle mass: particles with higher mass will have higher energy. The slope parameter is a measure of the particle energy induced by the transverse motion. Roughly speaking, the transverse motion contains both thermal (random) and collective modes. The intrinsic freeze-out temperature is determined by the thermal motion. For the p+p collisions, one does not expect any rescattering, and the slope parameter reflects the true freeze-out temperature. This is supported by the data since the slope parameters of pions, kaons, and protons are very similar, around 145 MeV for the p+p collisions. For heavy-ion collisions, rescattering becomes more important and collective motion gradually develops. The slope in the T vs mass plot indeed demonstrats such characteristic hydrodynamic behavior. Furthermore, due to multipole scatterings, is it necessary to consider the higher nuclear stopping and stronger hydro flow together for the heavy-system Pb+Pb collisions.

A few remarks should be made regarding Fig. 5:

mass $\geq$0.2 GeV.

- One may empirically guess a relationship between the slope parameter and particle mass:

$$T = T_{fo} + \mathrm{mass}\langle\beta\rangle^2,$$

where T_{fo} and $\langle\beta\rangle$ are the freeze-out temperature parameter and averaged collective flow velocity, respectively. This hydro behavior has also been used for analysis at few A·GeV heavy-ion collisions [25]. In reference [26], Csörgő and Lörstad discussed a similar relationship within a framework of a hydrodynamic model.[5] There, $\langle\beta\rangle$ is interpreted as the mean expansion velocity $\langle\beta\rangle = R_G/t_0$, where R_G and t_0 are geometrical radius and mean freeze-out time, respectively.

- Using the transport code RQMD, the transverse collective velocity profile can also be evaluated. For the Pb+Pb central collisions, we found that the velocity profiles of pion, kaon, and protons are very similar, indicating the onset of hydrodynamics in the cascade model. The maximum velocity is found to be about $0.6c$ and the average velocity is $0.43c$. This result plus the hadron freeze-out temperature extracted from the RQMD calculation [27] of 140 MeV are in good agreement with the above purely hydro approach.[6]

- Recently, Leonidov, Nardi, and Satz [28] proposed a mechanism of 'random walk initial state collisions' to explain the slope parameters extracted from heavy-ion induced central collisions. However, using this model, the slope parameters of pion, kaon, and proton cannot be reproduced consistently with a set of temperature T and 'broadening' δ_{AA} ($A =$S, Pb) parameters.

Hydrodynamical models have been successful in describing the space-time evolution of heavy-ion collisions from energies of a few hundred MeV per nucleon at the LBL Bevelac and GSI SIS to ultrarelativistic energies of a few tens and hundreds of GeV per nucleon at the BNL AGS and CERN SPS [29]-[38]. The experimentally measured transverse momentum distributions [36]-[38] are well reproduced by hydrodynamical calculations in which the thermal parameters, such as the freeze-out temperature and transverse velocity can be identified.

[5] A certain type of equation of state and conditions were used to reach this relationship. For more details see Ref. [26]

[6] The hadron freeze-out temperature of 140 MeV is true for both 200A·GeV S+S and 160A·GeV Pb+Pb collisions, in remarkable agreement with our result of Fig. 5.

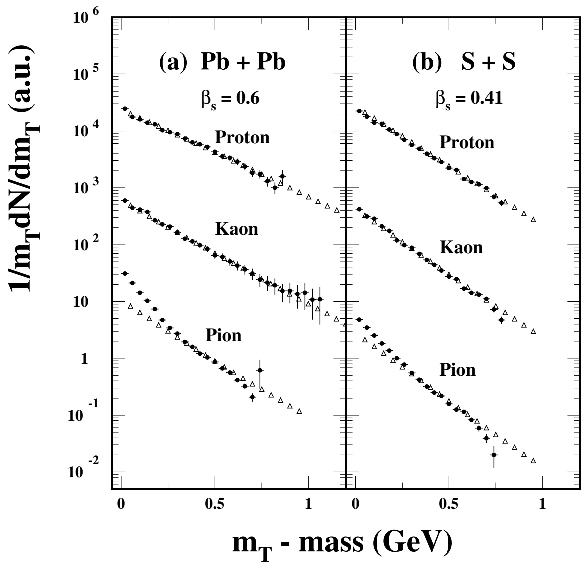

Figure 6. NA44 preliminary transverse momentum distributions for pions, kaons, and protons (dots) compared with results of a thermal model calculation (open triangles).

Details of the hydrodynamical model that we are going to use here can be found in Ref. [36]. With a velocity profile $\beta = \beta_s(r/R)^\alpha$ ($\alpha = 1$) and $T_{fo} = 140$ MeV, we calculated the transverse kinetic energy distributions of pions, kaons, and protons for both S+S and Pb+Pb central collisions. The results are compared with measurements in Fig. 6 where the experimental data are shown as dots and the model calculations are shown by the open triangles. It is clear that the overall fitting is good except for pions at the low p_T region where the resonance decays become important. When the resonance decays are included, a better fitting for pion spectra can be achieved [37]. The maximum (averaged) collective velocities are found to be $0.41c$ ($0.27c$) and $0.6c$ ($0.4c$) for S+S and Pb+Pb collisions, respectively. Typically the error on these values is 10%.

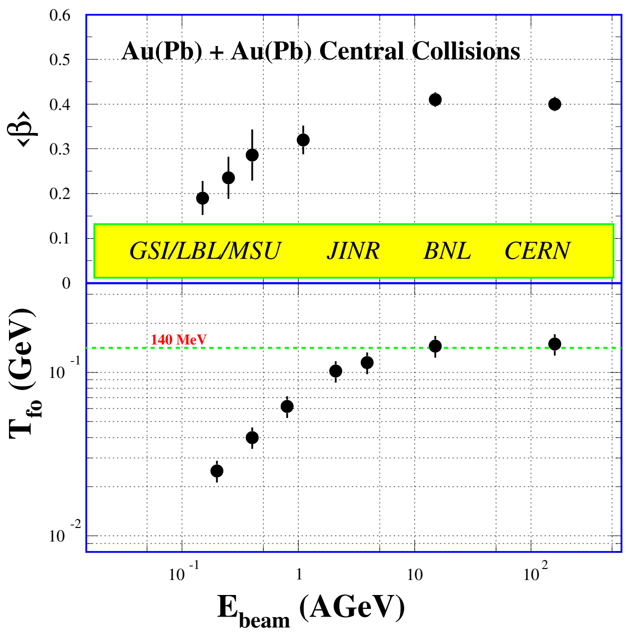

Figure 7. Freeze-out temperature parameter T_{fo} and averaged collective flow velocity $\langle\beta\rangle$ as a function of beam energy. Around E_{beam} $\approx$10 GeV, both quantities seem to be saturated.

As has been discussed, the freeze-out temperature T_{fo} and flow velocity $\langle\beta\rangle$ can be separated without any model-dependent analysis (see Fig. 5). It is worth noting that a plot similar to Fig. 5 can be found at the AGS energies ($E_{beam} \approx 10 - 15$A·GeV) [39]. It is especially interesting to see that the characteristic freeze-out temperature T_{fo} is also about 150 MeV! On the other hand, at lower energies, $E_{beam} \approx 0.2 - 5$A·GeV, one finds that T_{fo} increases dramatically as the beam energy increases [25,35,40–42]. Figure 7 shows the bombarding energy dependence of the freeze-out temperature T_{fo} and averaged collective velocity $\langle\beta\rangle$.[7] It is interesting to observe that both T_{fo} and $\langle\beta\rangle$ saturate at a beam energy about 10 A·GeV. The saturation temperature is about 145 MeV, very close to the mass of the lightest meson [43,44]. The steep rise of the T_{fo} up to about 5 GeV incident energy indicates that at low energy collisions the thermal energy essentially goes into heat. The saturation at ∼10 GeV shows that the generation of mass becomes important. As proposed in Refs. [43,45], for a pure hadron scenario there may be a limiting temperature $T_c \approx 140$ MeV in high-energy collisions, although the underline physics for both the hadronization, transition from a partonic to a hadronic degree of freedom, and the transition from interacting hadron to free-streaming hadron gas is not clear at the moment. By coupling the limiting temperature idea to a hydrodynamic model calculation, Stöcker *et al.* successfully predicted [46] the energy dependence in the freeze-out temperature.

The saturation in the transverse collective flow velocity (Fig. 7, top plot) indicates that as the bombarding energy increases, transverse motion will not increase any further. Rather, the momentum space in the longitudinal direction becomes larger.

3.4. Particle Ratios

Having fixed the freeze-out temperature parameter T_{fo} and the collective flow velocity $\langle\beta\rangle$, we now turn to the issue of particle ratios. Assuming chemical equilibrium, the chemical potentials (μ_q, μ_s) can be extracted from the measured particle ratios. The NA44 spectrometer can measure particles of both signs at the same p_T and y window. It is therefore a unique advantage for studying particle production ratios since many systematic errors will cancel out. In Fig. 8, the preliminary K^-/K^+ and $\bar{p}/p$ ratios are shown as a function of rapidity for both S+S and Pb+Pb central collisions. Model predictions of RQMD (v1.08) [47] and VENUS (v4.12) [48] are represented by dashed and solid lines, respectively. The systematic errors on the ratios for Pb+Pb collisions are estimated to be 15%. The main contributors to the rather large error bars are centrality determination and pion-veto corrections. For the S+S collisions, the systematic error is 11%.

In the case of the $\bar{p}/p$ ratio, both model predictions deviate from the data by a factor of 3 for the light colliding system S+S. For the Pb+Pb collisions, RQMD seems to give better results. However, for kaons, both model always overpredict the ratios. It is clear that much work has to be done in order to understand the details of the particle production in heavy-ion collisions.

[7] The error bars are statistical only. Due to several uncertainties involved, the systematic errors could be as large as 15%. In any case, this will not affect our main conclusions.

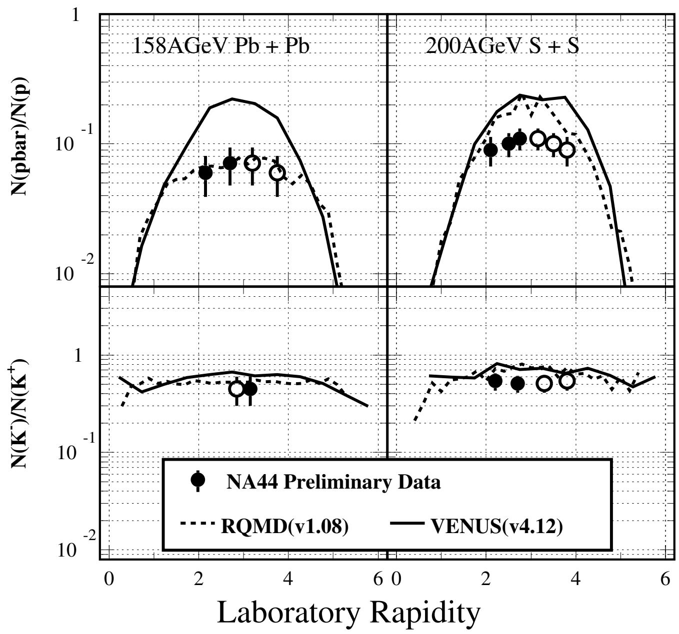

Figure 8. NA44 preliminary K^-/K^+ and $\bar{p}/p$ ratios. Open circles are mirrored about the central rapidity of 3.0 and 2.9 for S+S and Pb+Pb central collisions, respectively. RQMD and VENUS predictions are shown as dashed and solid lines, respectively.

4. SUMMARY

We have reported midrapidity proton rapidity densities from central Pb+Pb collisions at $\sqrt{s} = 17.5$A·GeV. A large number of protons are observed at midrapidity, indicating a high degree of nuclear stopping in the collision. This is consistent with the strong Coulomb effect observed recently by the NA44 collaboration [17] and the high energy density result from NA49 transverse energy measurements [49] in the Pb+Pb collisions. These are the direct consequences of high stopping and copious secondary particle production. In addition, due to the higher nuclear stopping in heavier system, the averaged transverse flow velocity is found to be increased from $0.27c$ to $0.41c$ for S+S and Pb+Pb central collisions, respectively. The systematics of the transverse momentum distributions of p+p, S+S, and Pb+Pb collisions strongly suggest a freeze-out temperature of $T_{fo} \approx 145 \pm 15$ MeV for collisions above a beam energy about 10 A·GeV. The measured particle ratios of K^-/K^+ and $\bar{p}/p$ decrease from the S+S to Pb+Pb central collisions, showing a characteristic of increasing baryon chemical potential. However, the current results of cascade models RQMD (v1.08) and VENUS (v4.12) cannot fully reproduce the observed particle ratios.

All of our discussions were based on the measured light hadrons at the freeze-out stage. If thermal and chemical equilibria are indeed reached, information on the earlier stage of the collision is lost. In order to gain insight into the initial condition of heavy-ion collisions, we need to investigate the distributions and yields of leptons and photons and possibly high mass multi-strange resonances as well.

Acknowledgements: The author wishes to express his thanks to Drs. G. Baym, G.E. Brown, T. Csörgő, E.L. Feinberg, M. Gyulassy, J. Kapusta, S. Pratt, B. Schlei, H. Sorge, and E. Shuryak for many helpful discussions on the physics of nuclear stopping and thermalization in heavy-ion collisions. We are grateful to the staff of the CERN PS-SPS accelerator complex for their excellent work. We thank the technical staff at CERN and the collaborating institutes for their valuable contributions. We are also grateful for the support given by the Austrian Fonds zur Foerderung der Wissenschaftlichen Forschung; the Science Research Council of Denmark; the Japanese Society for the Promotion of Science; the Ministry of Education, Science and Culture, Japan; the Science Research Council of Sweden; the National Science Foundation.

REFERENCES

1. H. Beker *et al.*, (The NA44 Collaboration), Phys. Lett. **B302**, 510(1993).
2. A. Franz, (The NA44 Collaboration), Quark Matter '96 Proceedings, May 1996.
3. M. Gyulassy, Nucl. Phys. **A590**, 431c(1995).
4. J. Bachler *et al.*, (NA35 Collaboration), Phys. Rev. Lett. **72**, 1419(1994).
5. D.S. Barton, *et al.*, Phys. Rev. **D27**, 2580(1983).
6. R.C. Hwa, Phys. Rev. Lett. **52**, 492(1984).
7. C.Y. Wong, Phys. Rev. Lett. **52**, 1393(1984).
8. L.P. Csernai and J.I. Kapusta, Phys. Rev. **D29**, 2664(1984), *ibid*, **D31**, 2795(1985).
9. W. Busza and A.S. Goldhaber, Phys. Lett. **B139**, 235(1984).
10. S. Datè, M. Gyulassy, and H. Sumiyoshi, Phys. Rev. **D32**, 619(1985).
11. H. Sorge *et al.*, Phys. Lett. **B289**, 6(1992).
12. B. Andersson *et al.*, Nucl. Phys. **B281**, 289(1987).
13. E.L. Feinberg, Soviet Phys., JETP, **23**,132(1966).
14. S. Jeon and J. Kapusta, private communication, May 1996.
15. J. Knoll and J. Randrup, Nucl. Phys. **A324**, 445(1979).
16. J. Hüfner and A. Klar, Phys. Lett. **B145**, 167(1984).
17. H. Bøggild *et al.*, (NA44 Collaboration), Phys. Lett. **B372**, 339(1996).
18. H. Bøggild *et al.*, (NA44 Collaboration), Z. Physik **C69**., 621(1996).
19. M. Gonin *et al.*, (E802/E866 collaboration), Nucl. Phys. **A566**, 601c(1994) and F. Videbæk *et al.*, (E802/E866 collaboration), Nucl. Phys. **A591**, 249c(1995).
20. J. Pluta, private communication, May 1996.
21. R. Lednický, V.L. Lyuboshitz, B. Erazmus, and D. Nouais, submitted to Nucl. Phys. **A**, June 1996.
22. H.W. Barz, J. Bondorf, and J.J. Gaardhøje, private communication, March 1996.
23. V. Koch, G.E. Brown, and C.M. Ko, Phys. Lett. **B265**, 29(1991); V. Koch, Nucl. Phys. **A591**, 531c(1995).
24. B. Alper *et al.*, Nucl. Phys. **B100**, 237(1975) and K. Guettler *et al.*, Nucl. Phys. **B116**, 77(1976).
25. N. Herrmann, Quark Matter '96 Proceedings, May 1996.
26. T. Csörgő and B. Lörstad, Phys. Rev. **C**, in press.
27. H. Sorge, Phys. Lett. **B**, in press.
28. A. Leonidov, M. Nardi, and H. Satz, CERN-TH/96-71 and this proceedings.
29. H. Stöcker and W. Greiner, Phys. Rep. **137**, 277(1986).
30. H.H. Gutbrod, A.M. Poskanzer, and H.G. Ritter, Rep. Prog. Phys. **52**, 1267(1989).
31. H.A. Gustaffson *et al.*, Phys. Rev. Lett., **52**, 1590(1984).

32. R.E. Renfordt *et al.*, Phys. Rev. Lett., **53**, 763(1984).
33. H. von Gersdorff, L.D. McLerran, M. Kataja, and P.V. Ruuskanen, Phys. Rev. **C34**, 794(1986), and M. Kataja, P.V. Ruuskanen, L.D. McLerran, and H. von Gersdorff, Phys. Rev. **C34**, 2755(1986).
34. U. Ornik, F.W. Pottag, and R.M. Weiner, Phys. Rev. Lett. **63**, 2641(1989), and U. Ornik and R.M. Weiner, Phys. Lett. **B263**, 503(1991).
35. M.A. Lisa *et al.*, Phys. Rev. Lett., **75**, 2662(1995).
36. E. Schnedermann, J. Sollfrank, and U. Heinz, Phys. Rev. **C48**, 2462(1993), and E. Schnedermann, J. Sollfrank, and U. Heinz, *'Particle Production in Highly Excited Matter,'* p.175, Ed. H. Gutbrod and J. Rafelski, Plenum Press, New York, 1992.
37. P. Braun-Munzinger, J. Stachel, J.P. Wessels, and N. Xu, Phys. Lett. **B344**, 43(1995), *ibid*, **B365**, 1(1996).
38. J. Dodd *et al.*, (NA44 Collaboration), Nucl. Phys. **A590**, 523c(1995) and B.V. Jacak *et al.*, (NA44 Collaboration), Nucl. Phys. **A590**, 215c(1995).
39. Z. Chen, (E802 Collaboration), BNL AGS Users Meeting, 1995; T. Abbott *et al.*, (E802 Collaboration), Phys. Rev. **C50**, 1024(1994); Z. Chen, I. J. Mod. Phys. E, **V2(2)**, 285(1993).
40. S. Nagamiya *et al.*, Phys. Rev. **C24**, 971(1981).
41. G. Poggi *et al.*, Nucl.Phys. **A586**, 755(1995).
42. A. Jipa, J. Phys. G: Nucl. Part. Phys., **V22(2)**, 231(1996).
43. I.Ya. Pomeranchuk, Dokl. Akad. Sci. U.S.S.R. **78**, 884(1951).
44. L.D.Landau, Izv. Akad. Nuak SSSR Ser. Fiz. 17, 51(1953).
45. R. Hagedorn, Suppl. Nuovo Cim. **III.2**, 147(1965).
46. H. Stöcker, A.A. Ogloblin, and W. Greiner, Z. Phys. **A303**, 259(1981).
47. H. Sorge, H. Stöcker, and W. Greiner, Ann. Phys. (NY) **192**, 266(1989); H. Sorge, Phys. Rev. **C52**, 3291(1995).
48. K. Werner, Phys. Rep. **232**, 87(1993).
49. T. Alber *et al.*, (NA49 Collaboration), Phys. Rev. Lett. **75**, 3814(1995).